

Rapid microcantilever-thickness determination by optical interferometry

This content has been downloaded from IOPscience. Please scroll down to see the full text.

2014 Meas. Sci. Technol. 25 015202

(<http://iopscience.iop.org/0957-0233/25/1/015202>)

View [the table of contents for this issue](#), or go to the [journal homepage](#) for more

Download details:

IP Address: 131.111.76.93

This content was downloaded on 06/12/2013 at 18:04

Please note that [terms and conditions apply](#).

Rapid microcantilever-thickness determination by optical interferometry

Andrew R Salmon¹, Matthew J Capener¹, Jeremy J Baumberg²
and Stephen R Elliott¹

¹ Department of Chemistry, University of Cambridge, Cambridge, CB2 1EW, UK

² NanoPhotonics Centre, Cavendish Laboratory, University of Cambridge, Cambridge, CB3 0HE, UK

E-mail: sre1@cam.ac.uk

Received 16 September 2013, revised 28 October 2013

Accepted for publication 4 November 2013

Published 4 December 2013

Abstract

Silicon microcantilevers are widely used in scanning-probe microscopy and in cantilever-sensing applications. However, the cantilever thickness is not well controlled in conventional lithography and, since it is also difficult to measure, it is the most important undefined factor in mechanical variability. An accurate method to measure this parameter is thus essential. We demonstrate the capability to measure microcantilever thicknesses rapidly (>1 Hz) and accurately (± 2 nm) by optical interferometry. This is achieved with standard microscopy equipment and so can be implemented as a standard technique in both research and in batch control for commercial microfabrication. In addition, we show how spatial variations in the thickness of individual microcantilevers can be mapped, which has applications in the precise mechanical calibration of cantilevers for force spectroscopy.

Keywords: interferometry, microcantilever calibration, microcantilever thickness, microcantilever sensing

 Online supplementary data available from stacks.iop.org/MST/25/015202/mmedia

(Some figures may appear in colour only in the online journal)

It is typical for commercial (silicon) microcantilevers to have a stated thickness (t) variability of 0.5–1 μm . This is a significant proportion of total microcantilever thicknesses (usually a few μm), and the mechanical properties, such as the force constant ($\propto t^3$) and resonant frequency ($\propto t$), are highly dependent on this parameter. Consequently these mechanical quantities are often poorly defined [1]. This is true even within a typical batch of cantilevers, originating from a single silicon wafer [2], and these thickness variations are the main source of mechanical variability in microcantilevers and microcantilever arrays [3].

This variation is a result of the manufacturing process which, in the case of silicon cantilevers, commonly involves lithographic processing of silicon-on-insulator (SOI) wafers [4]. The thickness of the silicon layer of SOI wafers, which defines the cantilever thicknesses, can vary substantially across a wafer [5]. Alternatively, silicon cantilevers can be fabricated using standard silicon wafers. In this case, the cantilever thickness is defined by a wet etch from one side of the wafer and is subject to thickness variations in the initial wafer.

Therefore either production method results in cantilever-thickness variations that are dependent on the original position of the cantilever on the source wafer.

Many ways have been developed to overcome these manufacturing limitations for applications in scanning-probe microscopy (SPM). In the case of standard atomic-force microscopy (AFM), it is routine to account for this variability by determining the resonant frequency of each individual cantilever. For some SPM techniques, such as force spectroscopy, more complex microcantilever calibration procedures are required and these need to be rapid, effective and efficient [6]. In this case, it is highly desirable to be able routinely to determine microcantilever thicknesses [7]. However, cantilever thicknesses are almost always determined using scanning electron microscopy (SEM) of edge-on sections, which is a slow process and is not accurate enough for resonant-frequency prediction [8].

In addition, there are applications for microcantilevers in fields other than SPM. In particular, the use of functionalized cantilevers as ‘chemical noses’ has been extensively reviewed

[4, 9, 10]. The basis of this application is that microcantilevers can be mechanically modified by analyte-binding-induced changes in surface stress. A wide variety of analytes can be studied in this manner including biologically relevant molecular structures, such as antibodies, enzymes and other proteins [11, 12]. Although the mechanical properties of the cantilevers are equally crucial for this application, the infrastructure generally used to account for cantilever variability in SPM (such as piezoelectric actuators) is not normally built into equipment. In special cases, where this infrastructure is built in, substantial variability has been found that necessitates calibration [13].

Because a wide variety of microcantilevers are used in microcantilever sensing, with different geometries and material properties [4], the cantilever responses cannot usually be directly compared. A standard way to interpret results for cantilever deflections is thus in terms of changes in the surface stress using Stoney's formula [14]:

$$\delta = \frac{3\Delta\sigma(1-\nu)L^2}{Et^2}, \quad (1)$$

where δ is the cantilever-tip deflection, $\Delta\sigma$ is the change in surface stress, ν is Poisson's ratio, L is the beam length and E is Young's modulus. This approach requires an accurate measurement of the cantilever thickness, t , because of the inverse quadratic dependence in equation (1) [3].

It is also common, particularly in biosensing experiments, to use a reference cantilever to take into account parasitic effects that can also cause the microcantilever to bend [15]. These include changes in temperature [16], changes in analyte medium refractive index [17] and non-specific binding [18]. By taking a differential signal between responses from measurement and reference cantilevers, these parasitic signals can be significantly reduced, but only provided the cantilevers are mechanically similar. Assessing the mechanical variability becomes even more important when using large microcantilever arrays made up of individual chips, as is becoming common in statistical cantilever biosensing [3, 19], where the variability between cantilevers on different chips can be much greater compared to that using a single cantilever on an array as a reference.

Here, we report a rapid, easy and precise method for determining the thicknesses of large numbers of microcantilevers using optical interferometry. While alternative interferometric approaches for determining cantilever thicknesses have been reported before [20, 21], to the best of our knowledge this is the first report both on cantilevers typical of SPM and cantilever sensing and with the large datasets increasingly integral to cantilever sensing. As a result, for the first time we are able to assess directly, and so potentially control for, the impact of thickness variability on the mechanical properties of microcantilevers. This quantification is achieved with standard optical-microscopy equipment and so can be readily and widely implemented as a standard technique.

The principle of the interferometry technique is that two reflections, in this case from the top and bottom interfaces of a microcantilever with the air, which are offset in phase by the difference in optical path length, are combined. When

Table 1. 'Typical' values of a range of mechanical parameters of Nanoworld Arrow TL2/TL2Au microcantilevers, according to the manufacturer's data.

Parameter	Typical values
Thickness	0.5–2.5 μm
Length	495–505 μm
Width	95–105 μm
Resonance frequency	3–14 kHz

a polychromatic light source is used, the intensity of the resulting reflection oscillates as a function of wavelength. A simple derivation (see supplementary information (available from stacks.iop.org/MST/25/015202/mmedia)) shows that the film thickness, t , is given by:

$$t = \frac{1}{2 \left[\left(\frac{n_1}{\lambda_1} \right) - \left(\frac{n_0}{\lambda_0} \right) \right]}, \quad (2)$$

where n_1 and n_0 are the refractive indices of the cantilever at the wavelengths λ_1 and λ_0 , respectively, which correspond to neighbouring intensity minima in the spectra.

This principle is widely exploited to determine film thicknesses, and here is used to determine the thicknesses of commercially acquired silicon-based cantilevers. Both uncoated and gold-coated silicon cantilevers (Nanoworld Arrow TL2/TL2Au) were used. These are tipless, rectangular microcantilevers with a triangular end and have the nominal parameters shown in table 1.

According to the manufacturer, each batch of 50 cantilever chips studied (corresponding to 100 cantilevers, as there are two cantilevers per chip) originates from the same wafer. The gold-coating of these TL2Au cantilevers consists of 30 nm of gold with a 5 nm titanium adhesion layer (manufacturer's data), deposited by evaporation. For brevity, the uncoated silicon and gold-coated silicon cantilevers will be referred to as Si and Au–Si cantilevers, respectively.

In order to apply equation (2) to determine the cantilever thicknesses, it is first necessary to establish a reliable model taking account of the refractive-index dispersion. This is done by simulating the spectra of Si and Au–Si cantilevers, with thicknesses in the range 1100–1400 nm, using a standard transfer-matrix method using the full complex dispersion of Si, Au and Ti. Having simulated the spectra, software was developed to find automatically all the spectral minima and to determine the cantilever thicknesses according to equation (2). For Si cantilevers, this analysis returned the simulated cantilever thicknesses from the spectra with an error of ± 1 nm.

For Au–Si cantilevers, it was necessary to adjust the refractive index used in order to determine correctly the cantilever thicknesses from the simulated spectra. To account for the full multilayer, equation (2) is rearranged to

$$\frac{d}{di} \frac{n_i}{\lambda_i} = \frac{1}{2t}. \quad (3)$$

Therefore, the derivatives of the $n_i\lambda_i^{-1}$ terms track the thickness and, as the values of the λ_i minima are also known, an 'effective' Au–Si cantilever refractive index can be extracted (up to a background constant that is not needed for

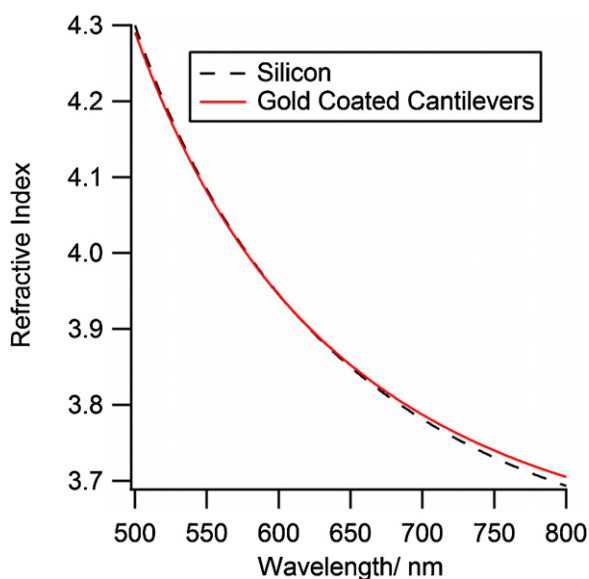
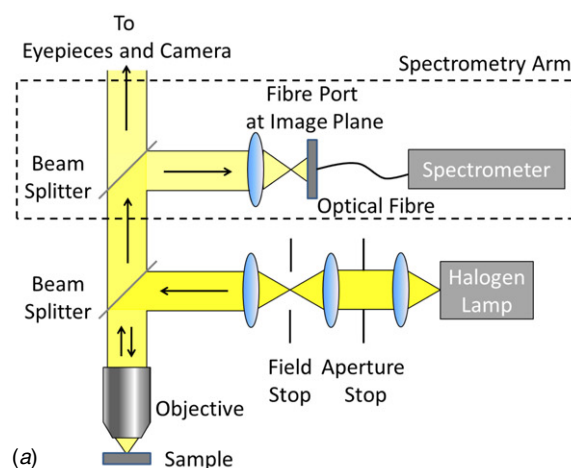


Figure 1. Refractive indices used for the thickness determination of Si and Au–Si cantilevers. In the case of Au–Si cantilevers, the refractive index shown corresponds to an ‘effective’ refractive index calibrated from simulated data, including phase shifts from the Au.

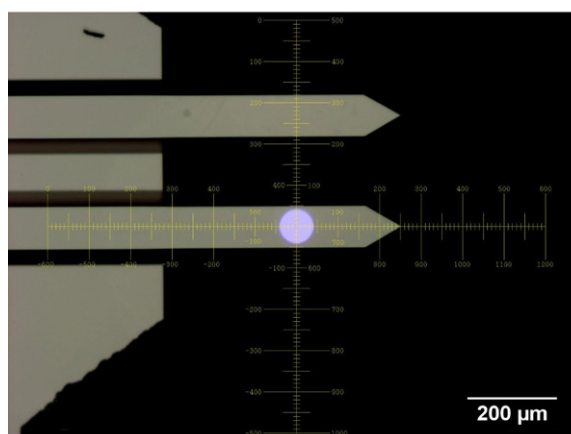
equation (2)). The dispersion of this refractive index is slightly modified compared to literature values for silicon (figure 1). Using this calibration, Au–Si cantilever thicknesses can be rapidly determined from the simulated spectra within an error of ± 2 nm.

Having calibrated the analysis with simulated data, interferometric measurements were performed by optical microscopy and spectroscopy on cantilevers using an Olympus BX51 optical microscope coupled to an Ocean Optics QE65000 spectrometer through an optical fibre (Ocean Optics QP200-2-VIS-NIR), such that spectra could be taken selectively from well-defined spatial regions on each given cantilever (figure 2(a)). Illuminating with light from the same optical fibre as used for spectral collection allowed the collection spot (marked in figure 2(b)) to be centred and aligned with the image focal plane. Areas of approximately the same spatial scale as the cantilever width were analysed, although spot sizes down to ~ 1 μm are easily achievable. As a result, in principle any cantilevers with length and width dimensions greater than this size are measurable.

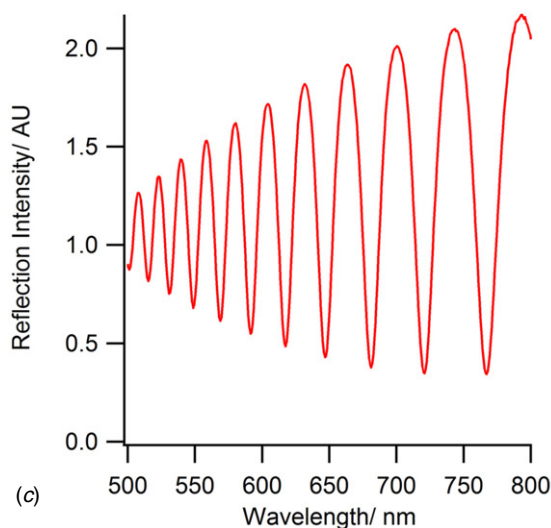
Spectroscopy was performed using a $5\times$ objective in bright-field mode, with a tungsten–halogen lamp as the incident light source. The geometry of this illumination allowed for analysis of cantilever chips without removal from their protective packaging, which is advantageous to minimize both sample contamination and damage. The signal from the cantilever-chip body was used as a reference to normalize the spectra, and resulted in clearly defined interference spectra (figure 2(c)). Gold-coated cantilevers were probed with the cantilevers being free hanging from the packaging, i.e. with the gold-coated side facing the microscope objective. Interferometric measurement in this geometry requires that the gold layer is thin enough to allow sufficient light to pass through it. Although this was not a restriction in this work, it is not unusual for microcantilevers to have relatively



(a)



(b)



(c)

Figure 2. (a) A schematic of the instrumentation used for optical interferometry. As described in the text, this is based upon a commercial reflected light microscope (Olympus BX51) with the addition of a spectrometry arm (boxed). (b) Bright-field microscope image of a Nanoworld Arrow TL2Au cantilever chip. The bright spot on one cantilever results from illumination by light from the same optical fibre as used for coupling to the spectrometer, and shows the ‘collection spot’ used for interferometric spectroscopy. (c) Normalized experimental interference spectrum from a Si cantilever.

thick (>50 nm) gold coatings. In these cases, it is possible to perform interferometric measurements with the silicon side facing the microscope objective. For convenience, the spectra can be recorded through transparent packaging, and data from 400 microcantilevers measured in this manner are included in the supplementary information (available from stacks.iop.org/MST/25/015202/mmedia).

Transfer-matrix calculations show that, with the instrumentation described, Si cantilevers could be measured in the thickness range 300 nm–20 μm . The limitation is the fringe spacing, which at low cantilever thickness becomes too wide for the spectral range. At high thickness, the fringe spacing is increasingly comparable to the experimental spectral resolution (1 nm), and so it would not be possible to resolve the fringes.

Commercial microcantilevers vary not only in thickness but also in length, width, shape and cross section. It has already been noted that provided the length and width are greater than 1 μm , the surface dimensions do not limit the applicability of the method described here. For cantilevers with a trapezoidal cross section, small spot sizes relative to the cantilever width could be used to ensure that, as equation (2) assumes, only areas with top and bottom faces perpendicular to the incident light are probed.

Preliminary results suggest that the interferometric thickness measurement also works for polymer-based cantilevers and, given the widespread use of interferometry in the determination of the thickness of spin-coated polymer layers, it should be widely applicable in this case also.

The interferometric analysis was automated using custom software, using the calibrated refractive indices and equation (2), and could be performed at rates of hundreds of spectra analysed per second on a standard PC. The limiting factor was the spectral data-collection rate, and thus this technique is very rapid compared to competitors such as SEM or resonance-frequency testing.

Manually collecting interference data for all 100 cantilevers in a batch takes 40 min. Thicknesses recorded in this way show excellent reproducibility (± 2 nm) between measurements taken over different days and with different spectrometers. The data-collection rate could be significantly increased to more than 100 cantilevers per minute if the cantilevers were at precisely defined locations or image recognition is used to identify cantilevers, allowing for automated stage-movement to be used. This could be easily achievable during the manufacturing process for batch-control purposes, for instance.

Comparison of the interferometric thickness with the fundamental resonance frequency (obtained using a VEECO Dimension 3100 Atomic Force Microscope) for Si and Au–Si cantilevers showed the expected linear trend (figure 3(a)), indicating that the thickness variation is the dominant factor affecting the microcantilever mechanical properties. Similarly, comparison with SEM-derived thickness data (Philips FEI FEG XL30) showed a good fit to the expected 1:1 thickness relationship (figure 3(b)).

The substantial errors ($\pm 3\%$) associated with the SEM thickness determination (figure 3(b)) are similar to those found

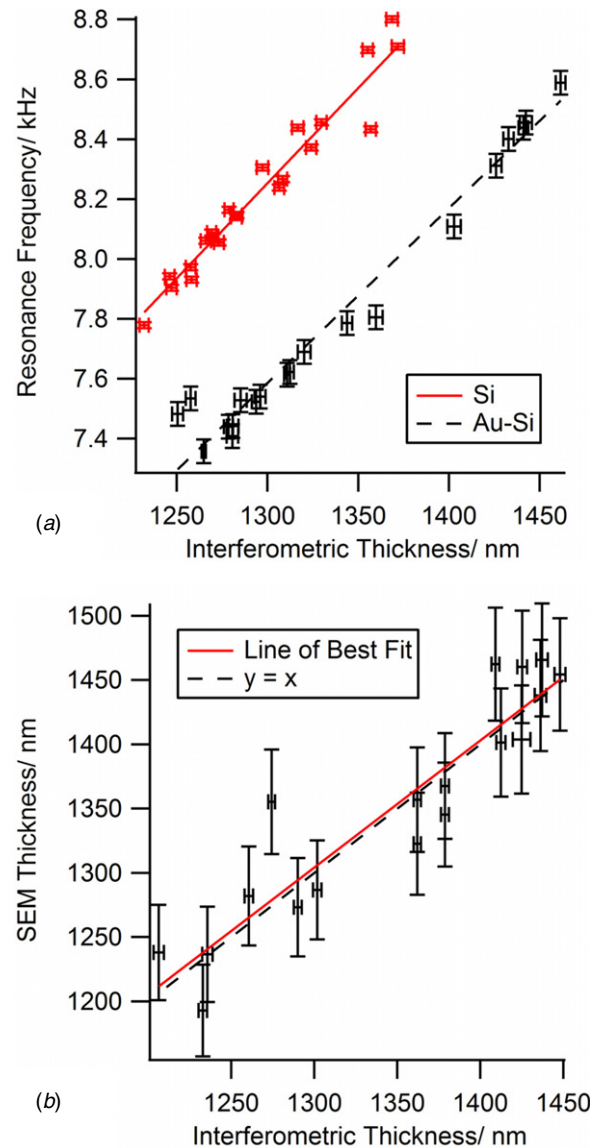


Figure 3. Comparison of interferometrically determined thicknesses of microcantilevers with data from (a) resonance-frequency testing and (b) SEM. Only Au–Si cantilevers are included in (b) as charging made the measurement of Si cantilevers by SEM problematic. Interferometric errors are given as the root-mean square of the thicknesses determined from each spectral peak pair.

in the literature [8] and are a consequence of the difficulty of accurately aligning cantilever edges with respect to the SEM image plane. The interferometry approach demonstrated here has clear advantages over SEM in terms of accuracy, expense and speed. Despite the substantial errors in the SEM-obtained thicknesses, the best-fit line matches well the interference-derived thickness determination.

The small deviations from the linear trend observed in the resonant-frequency data (figure 3(a)) are likely due to cantilever-length variations. The cantilever-length variation of 495–505 μm corresponds to a maximum variability in resonance frequency of 4%, which accounts for the deviations from the ideal thickness trend in these data. While cantilever-thickness variations are suggested to be the main cause of mechanical variability in applications such as cantilever

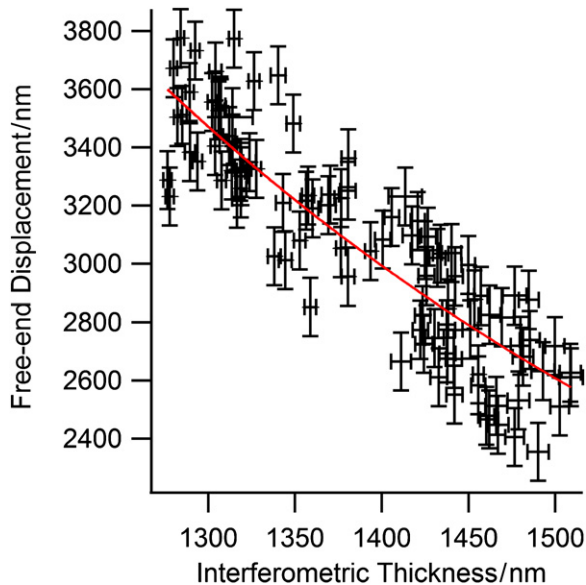


Figure 4. The ‘intrinsic’ free-end displacement of Au–Si cantilevers compared to the interferometric thicknesses. The free-end displacement is as a result of the surface stress from the Au–Ti layer applied to the silicon cantilevers by the manufacturer. This stress is assumed to be the same for all cantilevers. The measurement errors shown in the free-end displacement (i.e. the error bars) are a consequence of the uncertainty in determining the position of the cantilever end (red line is an inverse quadratic fit).

sensing [3], this does not appear to have been directly tested previously (although it is expected from the cantilever geometry). Presumably this is because accurate thickness data for statistically significant samples sizes were not previously available.

In order to address the issue of mechanical variability in cantilever sensing, we analysed the displacement profiles of a Au–Si cantilever batch (100 cantilevers) using phase-shifting interferometric microscopy [22]. The addition of gold–titanium layers onto the silicon cantilever surface induces a surface stress that results in a free-end displacement of these cantilevers, relative to the plane defined by the cantilever base. We make use of this ‘intrinsic’ displacement to examine the factors that affect the cantilever response variability.

Due to the different thermal-expansion coefficients of the Au and Si layers, the cantilever displacement is temperature dependent (a typical bimetallic effect) [23]. Here, the cantilevers were studied under ambient conditions (temperature 22.2 ± 0.8 °C, relative humidity $33.0\% \pm 3.2\%$).

From equation (1), the displacement of a cantilever due to an applied stress is proportional to the inverse square of the cantilever thickness, as is consistent with our displacement data (figure 4). The trend of the measured free-end displacement against the interferometric thickness also confirms that a significant cause of displacement variability is the cantilever thickness.

The relative importance of the thickness variation can be judged by comparing the standard deviation of the displacement values to the standard deviation of the displacement offset from the line of best fit (figure 4). By this

method, it is found here that the thickness variation accounts for 48% of the overall variability. The measurement error in displacement, assuming a normal distribution, accounts for another $\sim 15\%$. Using the manufacturer’s stated values, length variation can account for at most $\sim 8\%$, leaving $\sim 29\%$ of the overall variation to be accounted for.

Obvious contributory factors to the variation in displacement (figure 4) include variations in the temperature and humidity under the ambient conditions of measurement. However, both temperature and humidity were recorded for each data point and found to have no correlation with the deviation from the line of best fit. This indicates that neither temperature nor humidity are significant factors in the observed displacement variability. Similarly, there is no correlation between the fringe visibility and the deviation, and so variations in the thickness of the gold layer are also unlikely to be an important factor.

It has been previously reported that the ‘intrinsic’ displacement discussed here (in response to an applied gold layer) is highly sensitive to the conditions of deposition [24]. This is due to the local variations in surface nanostructure and chemical preparation, which we do not control here. Although the manufacturer would not reveal details of their evaporation procedure, except to say their method was consistent between cantilever batches, it is possible this could account for a degree of variation.

It is notable that the deviations from the line of best fit in figure 4 are much more significant than those observed in the resonance-frequency data (figure 3(a)). This would indeed be expected if the surface stress varied between samples, since the displacement ($\propto \Delta\sigma$) is more sensitive than the resonance frequency ($\propto \sqrt{\Delta\sigma}$) [25].

So far, all the cantilever thicknesses discussed have been for individual cantilevers, determined using a large collection spot relative to the cantilever width (figure 2(b)). It is also possible, using a smaller spot size, to analyse smaller areas within the width of a cantilever. Then, using an automated stage control, the collection spot can be moved relative to the sample, and cantilever ‘thickness images’ can be constructed (figure 5). The smaller spot size is achieved simply by using a collection fibre with a smaller ($50 \mu\text{m}$) core (Ocean Optics QP50-2-VIS-NIR) to give a spot size of $\sim 15 \mu\text{m}$ diameter, appreciably smaller than the cantilever width of $100 \mu\text{m}$ (figure 5(a)).

The data for figure 5 were collected in the form of a hyper-spectral cube, that is with two spatial dimensions and a third spectral dimension. The images then simply consist of a thickness value for each spatial pixel, derived from its associated spectrum.

These thickness images showed significant thickness variations within individual cantilevers (figures 5(b), (c)). Both Si and Au–Si cantilevers were measured to be ~ 100 nm thicker near the cantilever base than toward the free end, presumably due to etching inhomogeneities. Such spatial variations may help to explain the measurement error in SEM thickness determination (figure 3(b)) as well as the variations in Au–Si cantilever intrinsic displacements (figure 4).

As has already been discussed, the Au–Si cantilevers are intrinsically displaced downwards (for Au surfaces being

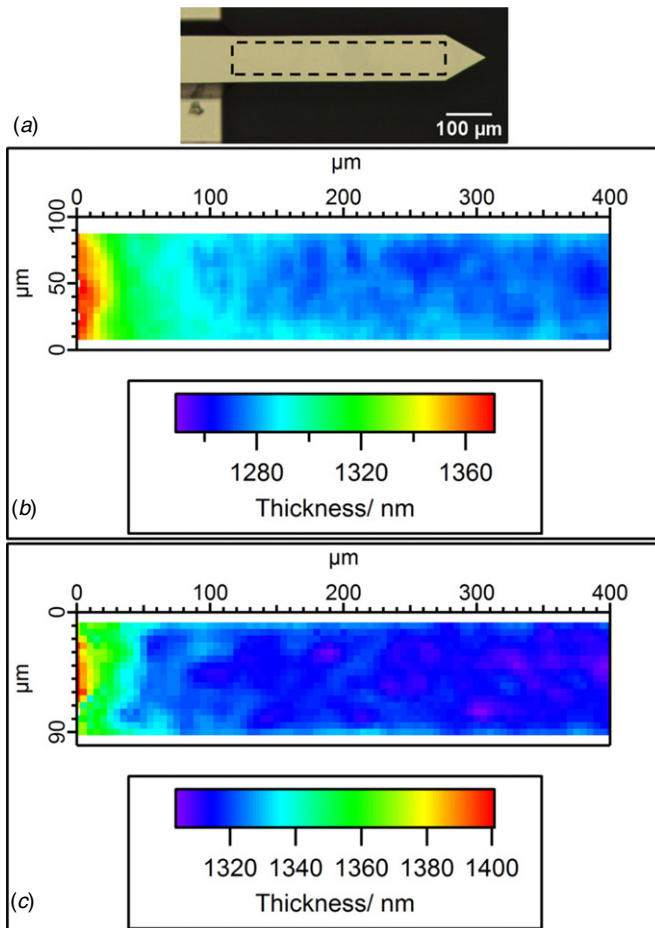


Figure 5. (a) A bright-field microscope image of a cantilever. The boxed area corresponds to the region sampled for a thickness map. (b) A thickness image of a Si cantilever, and (c) the same for a Au-Si cantilever. The thickness images were made using the interferometric method, together with a $15\ \mu\text{m}$ spot size and automated microscope-stage-movement, as described in the text.

uppermost) and they are therefore angled relative to the incident light. This is increasingly true towards the free end of the cantilevers where the displacement is a maximum. Equation (2), upon which the thickness measurement is based, assumes that the light is incident along the normal to the reflecting surfaces. Therefore, the possibility that this assumption is invalid, and that this angular-misalignment effect is responsible for the thickness trends shown in figures 5(b), (c), has to be addressed.

The possibility of the thickness variations in figure 5 being angle-related artefacts can be ruled out for two reasons. Firstly, the measured displacements of the Au-Si cantilevers only result in very small angular offsets relative to the cantilever bases, even at the cantilever free ends ($\sim 0.5^\circ$). Our transfer-matrix calculations show that this has a negligible impact on the thickness measured by the interferometric method. Secondly, uncoated Si cantilevers show the same thickness-map trends as for Au-Si cantilevers (figures 5(b), (c)), presumably due to variations in the processing of the Si cantilevers. We found that uncoated Si cantilevers have negligible intrinsic displacements relative to

Au-Si cantilevers. Therefore, the observed thickness trends conclusively cannot be displacement-related.

Thickness imaging of cantilevers is clearly more time consuming than performing a single thickness measurement, with the imaging data for a single cantilever taking ~ 30 min to collect, depending on the resolution. For this reason, it is probably not suited to the measurement of large arrays for cantilever sensing. However, it may have applications in precise single-cantilever work, such as force spectroscopy. Current calibration methods, such as the Sader method [26], often avoid requiring thickness as a parameter because accurate cantilever-thickness data have not previously been available. We have shown that it is not only possible to determine routinely the thicknesses of cantilevers, but also to determine the thickness-map profiles. This should greatly improve the accuracy of the geometric-calibration method, which is known to depend critically on the thickness determination [7]. In particular, thickness variations along cantilevers are known to have an effect on the cantilever static stiffness and dynamics [27, 28]. To the best of our knowledge, no other method of precisely characterizing such thickness variations has been reported.

With the greatly improved cantilever-thickness determination that we demonstrate, it is predicted that geometric calibration would be at least comparable to current force-constant calibration methods, which generally have uncertainties in the range 5–20% [6, 8]. By the geometric-calibration method, the uncertainty in the spring constant is reported to be 11% on account of the difficulty of determining the thickness and Young's modulus of a cantilever [8]. The stiffness uncertainty from thickness measurement error is reduced from $\sim 10\%$ to $\sim 1\%$ using the thickness determination we present here instead of using SEM. In addition, given the strong correlations we find between cantilever thickness and resonance frequency (figure 3(a)), it is clear that the variation in the Young's modulus is small. Consequently, given the convenience of the thickness determination method which we describe, geometric force-constant calibration requires reevaluation.

In summary, a rapid, reliable and non-contact interferometric method of establishing the thickness (with an accuracy of ± 2 nm) across whole microcantilever batches on a silicon wafer has been developed. Such a method would be useful for manufacturing batch control for the production of MEMS devices, as well as for cantilever-sensing research groups. On the basis of this work, it is predicted that the deflection of the cantilevers used here to an applied force will vary intrinsically by a factor of ~ 2 due to the measured thickness variations. This method is equally applicable to the measurements of large arrays of cantilevers designed for multiplexed sensing. In addition, we show that it is possible to construct thickness-image maps of cantilevers by this interferometric method. This could have significant implications in SPM applications that require precise mechanical calibration.

Acknowledgments

The authors wish to acknowledge the support of the UK Engineering and Physical Sciences Research Council

(EP/G060649/1, EP/G037221/1), the European Research Council (LINASS 320503), and both the Nano Doctoral Training Centre (NanoDTC) and the Nanophotonics group of the University of Cambridge.

References

- [1] Clifford C A and Seah M P 2009 Improved methods and uncertainty analysis in the calibration of the spring constant of an atomic force microscope cantilever using static experimental methods *Meas. Sci. Technol.* **20** 125501
- [2] Webber G B, Stevens G W, Grieser F, Dagastine R R and Chan D Y C 2008 Variations in properties of atomic force microscope cantilevers fashioned from the same wafer *Nanotechnology* **19** 105709
- [3] Kosaka P M, Tamayo J, Ruz J J, Puertas S, Polo E, Grazu V, de la Fuente J M and Calleja M 2013 Tackling reproducibility in microcantilever biosensors: a statistical approach for sensitive and specific end-point detection of immunoreactions *Analyst* **138** 863–72
- [4] Boisen A, Dohn S, Keller S S, Schmid S and Tenje M 2011 Cantilever-like micromechanical sensors *Rep. Prog. Phys.* **74** 036101
- [5] Selvaraja S, Rosseel E, Fernandez L, Tabat M, Bogaerts W, Hautala J and Absil P 2011 SOI thickness uniformity improvement using wafer-scale corrective etching for silicon nano-photonics device *Proc. 2011 Annu. Symp. of the IEEE Photonics Benelux Chapter* pp 289–92
- [6] Burnham N A, Chen X, Hodges C S, Matei G A, Thoreson E J, Roberts C J, Davies M C and Tendler S J B 2003 Comparison of calibration methods for atomic-force microscopy cantilevers *Nanotechnology* **14** 1–6
- [7] Luebke J, Doering L and Reichling M 2012 Precise determination of force microscopy cantilever stiffness from dimensions and eigenfrequencies *Meas. Sci. Technol.* **23** 045401
- [8] Clifford C A and Seah M P 2005 The determination of atomic force microscope cantilever spring constants via dimensional methods for nanomechanical analysis *Nanotechnology* **16** 1666–80
- [9] Goeders K M, Colton J S and Bottomley L A 2008 Microcantilevers: sensing chemical interactions via mechanical motion *Chem. Rev.* **108** 522–42
- [10] Lavrik N V, Sepaniak M J and Datskos P G 2004 Cantilever transducers as a platform for chemical and biological sensors *Rev. Sci. Instrum.* **75** 2229–53
- [11] Alvarez M and Lechuga L M 2010 Microcantilever-based platforms as biosensing tools *Analyst* **135** 827–36
- [12] Buchapudi K R, Huang X, Yang X, Ji H F and Thundat T 2011 Microcantilever biosensors for chemicals and bioorganisms *Analyst* **136** 1539–56
- [13] Martinez N F, Kosaka P M, Tamayo J, Ramirez J, Ahumada O, Mertens J, Hien T D, Rijn C V and Calleja M 2010 High throughput optical readout of dense arrays of nanomechanical systems for sensing applications *Rev. Sci. Instrum.* **81** 125109
- [14] Stoney G G 1909 The tension of metallic films deposited by electrolysis *Proc. R. Soc.* **82** 172–5
- [15] Zhang J, Lang H P, Huber F, Bietsch A, Grange W, Certa U, Mckendry R, Guntgerodt H J, Hegner M and Gerber C 2006 Rapid and label-free nanomechanical detection of biomarker transcripts in human RNA *Nature Nanotechnol.* **1** 214–20
- [16] Savran C A, Sparks A W, Sihler J, Li J, Wu W C, Berlin D E, Burg T P, Fritz J, Schmidt M A and Manalis S R 2002 Fabrication and characterization of a micromechanical sensor for differential detection of nanoscale motions *J. Microelectromech. Syst.* **11** 703–8
- [17] Mckendry R *et al* 2002 Multiple label-free biodetection and quantitative DNA-binding assays on a nanomechanical cantilever array *Proc. Natl Acad. Sci. USA* **99** 9783–8
- [18] Huber F, Lang H P, Backmann N, Rimoldi D and Gerber C 2013 Direct detection of a BRAF mutation in total RNA from melanoma cells using cantilever arrays *Nature Nanotechnol.* **8** 125–9
- [19] Bosco F G, Hwu E-T, Chen C-H, Keller S, Bache M, Jakobsen M H, Hwang I-S and Boisen A 2011 High throughput label-free platform for statistical bio-molecular sensing *Lab Chip* **11** 2411–6
- [20] Scholz T, Debski T, Barth W, Roemer F and Hillmer H 2006 A high-resolution optical study of cantilever heterostructure layer geometries *J. Micromech. Microeng.* **16** 2765–70
- [21] Reed J, Wilkinson P, Schmit J, Klug W and Gimzewski J K 2006 Observation of nanoscale dynamics in cantilever sensor arrays *Nanotechnology* **17** 3873–9
- [22] Kelling S, Paoloni F, Huang J Z, Ostanin V P and Elliott S R 2009 Simultaneous readout of multiple microcantilever arrays with phase-shifting interferometric microscopy *Rev. Sci. Instrum.* **80** 093101
- [23] Ramos D, Mertens J, Calleja M and Tamayo J 2007 Study of the origin of bending induced by bimetallic effect on microcantilever *Sensors* **7** 1757–65
- [24] Mertens J, Calleja M, Ramos D, Taryn A and Tamayo J 2007 Role of the gold film nanostructure on the nanomechanical response of microcantilever sensors *J. Appl. Phys.* **101** 034904
- [25] Ren Q and Zhao Y P 2004 Influence of surface stress on frequency of microcantilever-based biosensors *Microsyst. Technol.* **10** 307–14
- [26] Sader J E, Chon J W M and Mulvaney P 1999 Calibration of rectangular atomic force microscope cantilevers *Rev. Sci. Instrum.* **70** 3967–9
- [27] Sader J E, Sanelli J A, Adamson B D, Monty J P, Wei X, Crawford S A, Friend J R, Marusic I, Mulvaney P and Bieske E J 2012 Spring constant calibration of atomic force microscope cantilevers of arbitrary shape *Rev. Sci. Instrum.* **83** 103705
- [28] Frentup H and Allen M S 2011 Error in dynamic spring constant calibration of atomic force microscope probes due to nonuniform cantilevers *Nanotechnology* **22** 295703